Title	Internal shock model for the X-ray flares of Swift J1644+57
Author(s)	Wang, FY; Cheng, KS
Citation	Monthly Notices Of The Royal Astronomical Society, 2012, v. 421 n. 1, p. 908-912
Issued Date	2012
URL	http://hdl.handle.net/10722/149125
Rights	The definitive version is available at www.blackwell-synergy.com

Monthly Notices
of the
ROYAL ASTRONOMICAL SOCIETY

Mon. Not. R. Astron. Soc. **421,** 908–912 (2012) doi:10.1111/j.1365-2966.2012.20392.x

Internal shock model for the X-ray flares of Swift J1644+57

F. Y. Wang[1,2,3★] and K. S. Cheng[1★]

[1]*Department of Physics, University of Hong Kong, Pokfulam Road, Hong Kong, China*
[2]*Department of Astronomy, Nanjing University, Nanjing 210093, China*
[3]*Key Laboratory of Modern Astronomy and Astrophysics (Nanjing University), Ministry of Education, Nanjing 210093, China*

Accepted 2011 December 12. Received 2011 November 29; in original form 2011 October 3

ABSTRACT

Swift J1644+57 is an unusual transient event, likely powered by the tidal disruption of a star by a massive black hole. Multiple short time-scale X-ray flares were seen over a span of several days. We propose that these flares could be produced by internal shocks. In the internal shock model, the forward and reverse shocks are produced by collisions between relativistic shells ejected from a central engine. The synchrotron emission from the forward and reverse shocks could dominate in two quite different energy bands; under some conditions, the relativistic reverse shock dominates the X-ray emission and the Newtonian forward shock dominates the infrared and optical emission. We show that the spectral energy distribution of Swift J1644+57 could be explained by an internal shock model.

Key words: radiation mechanisms: non-thermal – X-rays: general.

1 INTRODUCTION

Swift J1644+57 was triggered by the *Swift* Burst Alert Telescope (BAT) on 2011 March 28 (Cummings et al. 2011). Swift J1644+57 was initially discovered as a long-duration gamma-ray burst (GRB 110328A) by the *Swift* satellite, but the light curve soon showed that it was quite different. It remained bright and highly variable for a long period and re-triggered the BAT three times over the next 48 h (Sakamoto et al. 2011). The isotropic X-ray luminosity of Swift J1644+57 ranges from 10^{45}–4×10^{48} erg s^{-1} and the total isotropic energy is about 3×10^{53} erg during the first 30 d after the BAT trigger (Burrows et al. 2011). From the strong emission lines of hydrogen and oxygen, Levan et al. (2011) estimate that the redshift of Swift J1644+57 is $z = 0.35$. From astrometric observations of the X-ray, optical, infrared and radio transients with the light-centroid of the host galaxy, it is found that the position of this source is consistent with its arising in the nucleus of the host galaxy (Bloom et al. 2011; Zauderer et al. 2011).

The X-ray light curve of Swift J1644+57 exhibits repeated extremely short time-scale flares. The flares have rise times as short as 100 s (Burrows et al. 2011). These flares are similar to the flares discovered in the gamma-ray burst (GRB) afterglow (Burrows et al. 2005), which may indicate the same origin. The internal shock model can produce the X-ray flares observed in GRB afterglows (Burrows et al. 2005; Fan & Wei 2005; Zhang et al. 2006; Yu & Dai 2009).

After Swift J1644+57 was discovered, several models were proposed to explain it, most of them concentrating on the idea that a main-sequence star was tidally disrupted by passing too close to a 10^6–10^7 $M_\odot$ black hole (Bloom et al. 2011; Burrows et al. 2011; Cannizzo, Troja & Lodato 2011; Shao et al. 2011; Socrates 2011). Krolik & Piran (2011) suggest that this event may be produced by a white dwarf tidally disrupted by a 10^4-$M_\odot$ black hole. The process is as follows: a star is disrupted as it passes near a supermassive black hole and much of its mass is distributed into an accretion disc around the black hole. A powerful jet is then launched. In these models, the X-ray emission is thought to be produced by external inverse Compton (EIC: Bloom et al. 2011) or synchrotron emission (Burrows et al. 2011). On the high-frequency side, however, the *Fermi* Large Area Telescope (LAT: Campana et al. 2011) and Very Energetic Radiation Imaging Telescope Array System (VERITAS: Aliu et al. 2011) upper limits require that the synchrotron self-Compton (SSC) component is suppressed by γ–γ pair production. The soft photons of γ–γ pair production are thought to be generated from thermal emission of the accretion disc or the disc outflow. In the SSC model, soft photons originating from thermal emission of the accretion disc may not provide an efficient source for γ–γ production. Because the condition of γ–γ production is $E_X E_\gamma (1 - \cos\theta) \geq 2(m_e c^2)^2$, where θ is the angle between the directions of the soft seed photon and the high-energy photon, only a fraction of high-energy emission can be absorbed by soft photons. Thus soft photons from the disc outflow may provide a better candidate (Strubbe & Quataert 2009). In the synchrotron emission model, the jet must have a strong magnetic field (Poynting-flux-dominated) and have ongoing *in situ* acceleration of electrons (Aliu et al. 2011; Burrows et al. 2011).

In this paper, we use the internal shock model to explain the X-ray flares of Swift J1644+57. An internal shock produces the prompt emission of a GRB in the standard fireball model (Paczyński & Xu 1994; Rees & Mészáros 1994). The internal shock model is also the leading model of X-ray flares in GRBs; in the external shock model it is very hard to account for X-ray flares (Burrows et al. 2005;

★E-mail: fayinwang@nju.edu.cn (FYW); hrspksc@hkucc.hku.hk (KSC)

Fan & Wei 2005). The central engine of this event may be formed as follows. When a supermassive black hole tidally disrupts a star, a disc is formed. A magnetic field may be produced through disc instability. The disc can then anchor and amplify the seed magnetic field to a strong ordered poloidal field, which in turn threads the black hole with debris material in the inner region of the disc. A large amount of rotational energy of the black hole can be extracted via the Blandford–Znajek (BZ) process, which creates a jet along the rotation axis (Blandford & Znajek 1977). The magnetic field lines will break the disc into blobs, so that many shells may be ejected (Cheng & Lu 2001). When a fast shell catches up with an early slow shell, an internal shock is generated. Other models of the central engine are also discussed, such as episodic accretion on to a central object due to a chopped accretion disc (Perna, Armitage & Zhang 2006) or episodic accretion due to modulation of the accretion flow by a magnetic barrier (Proga & Zhang 2006).

The structure of this paper is as follows. In the next section, we describe the dynamics of an internal shock arising from a collision between two shells and synchrotron radiation of the shocked electrons. In Section 3, we apply the model to Swift J1644+57. Finally, a summary is given in Section 4.

2 THE INTERNAL SHOCK MODEL

The internal shock model has been extensively discussed in the literature (Rees & Mészáros 1994; Paczyński & Xu 1994; Yu & Dai 2009; Yu, Wang & Dai 2009). We give a brief description of our model as follows. Shells with different Lorentz factors and densities are ejected by the central black hole. Collisions of a pair of ejecta can produce different intensities of X-rays. For example, two shells with similar Lorentz factor and density will produce a weak flare whereas two shells with large differences can produce a strong flare. Since the collision frequency of these pairs (internal shocks) should be very high, this should result in rapidly variable intensities. Simultaneously, some fast-moving shells ejected earlier can reach the interstellar medium (ISM) and produce an external shock there (Sari & Piran 1995). The earlier ejected shells are fewer and hence the radiation results from the external shock should be weak at the beginning. However, after collisions of pairs they can merge and move toward the ISM and provide more energy to the external shock. Therefore the radiation intensity due to the external shock should gradually increase. We note that since the injected energy provided in this way is discrete in form, the flux will increase substantially but gradually decrease back to the original light curve. This phenomenon is similar to that observed in GRBs and known as the 're-brightening' effect (Zhang & Mészáros 2002; Huang, Cheng & Gao 2006). In Fig. 1 we provide a schematic illustration of our model.

2.1 Shock dynamics

At a time $t_{\rm A}$, the central engine ejects a shell denoted as 'shell A' with bulk Lorentz factor $\gamma_{\rm A}$ and isotropic kinetic energy luminosity $L_{\rm A}$. Some time (δt) later, another shell B with $\gamma_{\rm B}$ and $L_{\rm B}$ is assumed to be ejected. In order to let shell B catch up and collide with shell A, $\gamma_{\rm B} > \gamma_{\rm A}$ is required. At radius $R_{\rm col} = \beta_{\rm A}\beta_{\rm B}c\delta t/\psi(z)(\beta_{\rm B} - \beta_{\rm A})$, a collision between A and B takes place. For $(\gamma_{\rm A}, \gamma_{\rm B}) \gg 1$, the collision radius is (Yu & Dai 2009)

$$R_{\rm col} \simeq \frac{2\gamma_{\rm A}^2 c\delta t}{[1-(\gamma_{\rm A}/\gamma_{\rm B})^2]\psi(z)}, \quad (1)$$

where $\psi(z) = 1 + z$.

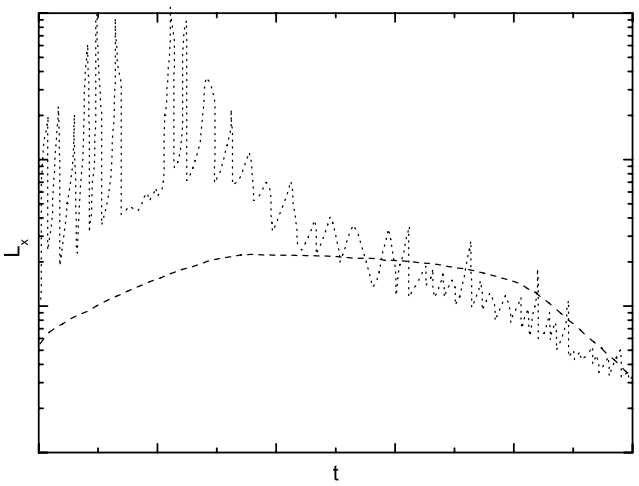

Figure 1. Schematic illustration of the model. The dotted line represents the intensity produced by internal shocks. The dashed line represents the intensity produced by the external shock. In this figure we argue that large short-term fluctuations can still occur, due to collisions of later ejecta when the jet still exists.

After the collision, a forward shock and a reverse shock are produced. The system is separated into four regions by the two shocks and a contact discontinuity surface: (1) unshocked shell A, (2) shocked shell A, (3) shocked shell B and (4) unshocked shell B, bulk Lorentz factors of which are $\gamma_1 = \gamma_{\rm A}$, $\gamma_2 = \gamma_3 \equiv \gamma$ and $\gamma_4 = \gamma_{\rm B}$. Two relative Lorentz factors of the shocked regions relative to unshocked regions 1 and 4 can be calculated by

$$\gamma_{21} = \frac{1}{2}\left(\frac{\gamma_1}{\gamma} + \frac{\gamma}{\gamma_1}\right), \quad \gamma_{34} = \frac{1}{2}\left(\frac{\gamma}{\gamma_4} + \frac{\gamma_4}{\gamma}\right). \quad (2)$$

According to Blandford & McKee (1976), the internal energy densities of the two shocked regions are $e_2 = (\gamma_{21}-1)(4\gamma_{21}+3)n_1 m_{\rm p}c^2$ and $e_3 = (\gamma_{34}-1)(4\gamma_{34}+3)n_4 m_{\rm p}c^2$, where $n_1 = L_{\rm A}/4\pi R_{\rm col}^2\gamma_{\rm A}^2 m_{\rm p}c^3$ and $n_4 = L_{\rm B}/4\pi R_{\rm col}^2\gamma_{\rm B}^2 m_{\rm p}c^3$. The mechanical equilibrium between the two shocked regions requires $e_2 = e_3$, so

$$\frac{(\gamma_{21}-1)(4\gamma_{21}+3)}{(\gamma_{34}-1)(4\gamma_{34}+3)} = \frac{n_4}{n_1} = \left(\frac{L_4}{L_1}\right)\left(\frac{\gamma_1}{\gamma_4}\right)^2 \equiv f, \quad (3)$$

where $L_1 = L_{\rm A}$ and $L_4 = L_{\rm B}$. We can calculate the values of γ, γ_{21} and γ_{34} from equations (2) and (3) after the parameters of the shells are given. In the four limiting cases, these equations can be solved analytically (Yu & Dai 2009). For $\gamma_4 \gg \gamma_1$,

(1) if $L_4/L_1 \gg (1/7)(\gamma_4/\gamma_1)^4$ then we have $\gamma_{21} = \gamma_4/2\gamma_1 \gg 1$, $\gamma_{34} - 1 \approx \gamma_4^2/7f\gamma_1^2$ and $\gamma = \gamma_4(1-\sqrt{2\xi})$, which means the forward shock is relativistic and the reverse shock is Newtonian;

(2) if $16 \ll L_4/L_1 \ll (1/16)(\gamma_4/\gamma_1)^4$ then we can obtain $\gamma_{21} = f^{1/4}\gamma_4^{1/2}/2\gamma_1^{1/2} \gg 1$, $\gamma_{34} = \gamma_4^{1/2}/2f^{1/4}\gamma_1^{1/2} \gg 1$ and $\gamma = f^{1/4}\gamma_1^{1/2}\gamma_4^{1/2}$, so both the two shocks are relativistic;

(3) if $L_4/L_1 \ll 7$ then we obtain $\gamma_{21} - 1 \approx f\gamma_4^2/7\gamma_1^2 = \xi$, $\gamma_{34} = \gamma_4/2\gamma_1$ and $\gamma = \gamma_1(1+\sqrt{2\xi})$, so the forward shock is Newtonian and the reverse shock is relativistic.

Finally,

(4) for $\gamma_4 \approx \gamma_1$ both the two shocks are Newtonian.

Since γ_1, γ_4, and f are unchanged with the moving of the shells, the values of γ ,γ_{21} and γ_{34} are constant before the shocks cross the shells (Yu & Dai 2009).

2.2 Synchrotron emission from forward and reverse shocks

Following Dai & Lu (2002), the total number of electrons swept-up by the forward and reverse shocks during a period δt can be expressed by $N_{\rm e,2} = 2\sqrt{2\xi}L_{\rm A}\delta t/\left(\psi(z)\gamma_1 m_{\rm p}c^2\right)$ and $N_{\rm e,3} = L_{\rm B}\delta t/\left(\psi(z)\gamma_4 m_{\rm p}c^2\right)$, respectively (Yu et al. 2009).

The forward and reverse shocks can accelerate particles to high energies. Following Sari, Piran & Narayan (1998), we assume that the energies of the hot electrons and magnetic fields are fractions $\epsilon_{\rm e}$ and ϵ_B of the total internal energy, respectively. Thus, the strength of the magnetic fields is $B_i = \left(8\pi\epsilon_{B,i}e_i\right)^{1/2}$, $i = 2, 3$. We assume a power-law distribution of the shock-accelerated electrons, $\mathrm{d}n_{\rm e}/\mathrm{d}\gamma_{\rm e} \propto \gamma_{\rm e}^{-p}$ for $\gamma_{\rm e} \geq \gamma_{{\rm e},m}$ (Sari et al. 1998). The random Lorentz factor of electrons in regions 2 or 3 is determined by

$$\gamma_{{\rm e},m,i} = \epsilon_{{\rm e},i}\frac{m_{\rm p}}{m_{\rm e}}\frac{(p-2)}{(p-1)}(\Gamma - 1),$$

where Γ equals γ_{21} or γ_{34}. In both shocked regions, the hot electrons with energies above $\gamma_{{\rm e},c,i}m_{\rm e}c^2$ lose most of their energies during a cooling time δt, where the cooling Lorentz factor is determined by $\gamma_{{\rm e},c,i} = 6\pi m_{\rm e}c\psi(z)/\left(\sigma_{\rm T}B_i^2\gamma\delta t\right)$. The two characteristic frequencies and a peak flux density are (Sari et al. 1998; Wijers & Galama 1999)

$$\begin{aligned}
\nu_{m,i} &= \frac{q_{\rm e}}{2\pi m_{\rm e}c\psi(z)}B_i\gamma_{{\rm e},m,i}^2\gamma,\\
\nu_{c,i} &= \frac{q_{\rm e}}{2\pi m_{\rm e}c\psi(z)}B_i\gamma_{{\rm e},c,i}^2\gamma,\\
F_{\nu,{\rm max},i} &= \frac{3\sqrt{3}\Phi(p)\psi(z)N_{{\rm e},i}m_{\rm e}c^2\sigma_{\rm T}B_i\gamma}{32\pi^2 q_{\rm e}d_{\rm L}^2},
\end{aligned} \tag{4}$$

where

$$d_{\rm L} = c(1+z)/H_0\int_0^z\frac{\mathrm{d}z'}{\sqrt{\Omega_{\rm M}(1+z')^3+\Omega_\Lambda}}$$

is the luminosity distance of the source and $\Phi(p)$ is a function of p, for $p = 2.2$, $\Phi(p) \approx 0.6$ (Wijers & Galama 1999). In the calculation, we use $\Omega_{\rm M} = 0.3$, $\Omega_\Lambda = 0.7$ and $H_0 = 70\,\mathrm{km\,s^{-1}\,Mpc^{-1}}$. $q_{\rm e}$ is the electron charge and $\sigma_{\rm T}$ is the Thomson cross-section. The synchrotron spectrum can be written as (Sari et al. 1998)

$$F_{\nu,i} = F_{\nu,{\rm max},i}\times\begin{cases}\left(\dfrac{\nu}{\nu_{\rm l}}\right)^{1/3}, & \nu < \nu_{\rm l},\\ \left(\dfrac{\nu}{\nu_{\rm l}}\right)^{-(q-1)/2}, & \nu_{\rm l} < \nu < \nu_{\rm h},\\ \left(\dfrac{\nu_{\rm h}}{\nu_{\rm l}}\right)^{-(q-1)/2}\left(\dfrac{\nu}{\nu_{\rm h}}\right)^{-p/2}, & \nu_{\rm h} < \nu,\end{cases} \tag{5}$$

where $\nu_{\rm l} = \min(\nu_{m,i}, \nu_{c,i})$, $\nu_{\rm h} = \max(\nu_{m,i}, \nu_{c,i})$ and $q = 2$ for $\nu_{c,i} < \nu_{m,i}$ and $q = p$ for $\nu_{c,i} > \nu_{m,i}$.

3 IMPLICATION FOR SWIFT J1644+57

There are two peaks in the spectrum of Swift J1644+57, far-infrared (FIR) and hard X-ray peaks. In order to fit the spectrum, we focus on case (3) of the internal shock model in section 2.1, in which the reverse shock is relativistic and the forward shock is Newtonian. In the rest of the paper we denote $Q = 10^x Q_x$. For illustration purposes, we set $L_4 = L_1 = L = 10^{47.0}\,\mathrm{erg\,s^{-1}}$, $\gamma_4 = 1000$, $\gamma_1 = 10$, $\epsilon_{\rm e,2} = \epsilon_{\rm e,3} = \epsilon_{\rm e} = 0.5$ and $\epsilon_{B,2} = \epsilon_{B,3} = \epsilon_B = 0.1$. As shown in Cheng & Lu (2001), the Lorentz factor of the shell can be up to 1000. It is reasonable to adopt $\gamma_4 = 1000$. According to observations, we use $\delta t \sim 100\,\mathrm{s}$, the variability time-scale of the flare (Bloom et al. 2011; Burrows et al. 2011). The collision radius is $R_{\rm col} \sim 2\gamma_1^2 c\delta t/\psi(z) \sim 5\times10^{14}\,\mathrm{cm}$, which is consistent with the X-ray emission radius determined from observations (Bloom et al. 2011). The Lorentz factor of the merged shell is $\gamma \sim 14$. Using equation (4), we can obtain the following expressions for the reverse shock:

$$\begin{aligned}
\nu_{m,3} &\simeq 1.2\times10^{18}\,\mathrm{Hz}\,\epsilon_{\rm e,-0.3}^2\gamma_{4,3}^2L_{47}^{1/2}\epsilon_{B,-1}^{1/2}\delta t_2^{-1}\gamma_{1,1}^{-4},\\
\nu_{c,3} &\simeq 2.2\times10^{13}\,\mathrm{Hz}\,L_{47}^{-3/2}\epsilon_{B,-1}^{-3/2}\delta t_2\gamma_{1,1}^8,\\
F_{\nu,{\rm max},3} &\simeq 0.9\,\mathrm{mJy}\,L_{47}^{3/2}\epsilon_{B,-1}^{1/2}\gamma_{1,1}^{-2}\gamma_{4,3}^{-1}d_{\rm L,27.7}^{-2}.
\end{aligned} \tag{6}$$

For the forward shock, we obtain

$$\begin{aligned}
\nu_{m,2} &\simeq 3.5\times10^{11}\,\mathrm{Hz}\,\epsilon_{\rm e,-0.3}^2L_{47}^{1/2}\epsilon_{B,-1}^{1/2}\delta t_2^{-1}\gamma_{1,1}^{-2},\\
\nu_{c,2} &\simeq 2.2\times10^{13}\,\mathrm{Hz}\,L_{47}^{-3/2}\epsilon_{B,-1}^{-3/2}\delta t_2\gamma_{1,1}^8,\\
F_{\nu,{\rm max},2} &\simeq 15\,\mathrm{mJy}\,L_{47}^{3/2}\epsilon_{B,-1}^{1/2}\gamma_{1,1}^{-3}d_{\rm L,27.7}^{-2}.
\end{aligned} \tag{7}$$

Therefore, the resulting synchrotron photons emitted by the two shocks are expected to peak in two different energy bands and thus provide two distinct spectral components.[1] The peak of the reverse shock spectrum will be at hard X-ray frequencies, but the peak of the forward shock will be at FIR frequencies. The synchrotron self-absorption must be taken into account. In the case $\nu_{m,2} < \nu_{a,2} < \nu_{c,2}$, the synchrotron self-absorption frequency in region 2 reads (Panaitescu & Kumar 2000)

$$\begin{aligned}
\nu_{a,2} &= \left(\frac{5q_{\rm e}N_{\rm e,2}}{4\pi R_{\rm col}^2B_2\gamma_{{\rm e},m,2}^5}\right)^{2/(p+4)}\nu_{m,2}\\
&\simeq 6.0\times10^{12}\,\mathrm{Hz}\,\epsilon_{\rm e,-0.3}^{\frac{2p-2}{p+4}}L_{47}^{\frac{6+p}{2(p+4)}}\epsilon_{B,-1}^{\frac{p+2}{2(p+4)}}\gamma_{1,1}^{-\frac{12+2p}{p+4}}.
\end{aligned} \tag{8}$$

In the case $\nu_{a,3} < \nu_{c,3} < \nu_{m,3}$, the synchrotron self-absorption frequency in region 3 can be calculated by (Panaitescu & Kumar 2000)

$$\begin{aligned}
\nu_{a,3} &= \left(\frac{5q_{\rm e}N_{\rm e,3}}{4\pi R_{\rm col}^2B_3\gamma_{e,c,3}^5}\right)^{3/5}\nu_{c,3}\\
&\simeq 1.0\times10^{13}\,\mathrm{Hz}\,\epsilon_{B,-1}^{6/5}L_{47}^{8/5}\gamma_{4,3}^{-3/5}\gamma_{1,1}^{-38/5}\delta t_2^{-2}.
\end{aligned} \tag{9}$$

The maximum Lorentz factor is limited by the synchrotron losses and is given by (Cheng & Wei 1996)

$$\gamma_{{\rm M},i} \simeq (3q_{\rm e}/B_i\sigma_{\rm T})^{1/2} \simeq 4\times10^7B_i^{-1/2}. \tag{10}$$

Another mechanism to restrict the maximum energy of an electron is diffusion. It turns out that the maximum Lorentz factor restricted by diffusion is much larger than that in equation (10). The maximal synchrotron photon energy can therefore be estimated (Fan & Piran 2008) as

$$h\nu_{{\rm M},i} \simeq \frac{hq_{\rm e}B_i}{2\pi m_{\rm e}c\psi(z)}\gamma_{M,i}^2\Gamma \sim \frac{30\Gamma}{1+z}\,\mathrm{MeV}, \tag{11}$$

where h is the Planck constant and Γ equals γ_{21} or γ_{34}.

The spectrum of the internal shock model is shown in Fig. 2 using the above parameters during a high state. The X-ray spectrum of Swift J1644+57 can be generated in our model. A moderate extinction ($A_V \sim 3$–5) is required to explain the spectrum. This value

[1] We can see that the characteristic frequencies ν_c and ν_m are very sensitive to the Lorentz factor. However, Kobayashi, Piran & Sari (1997) have shown that the radiation loss is less than 10 per cent of the total energy, therefore there is virtually no evolution of these spectral parameters during the collision.

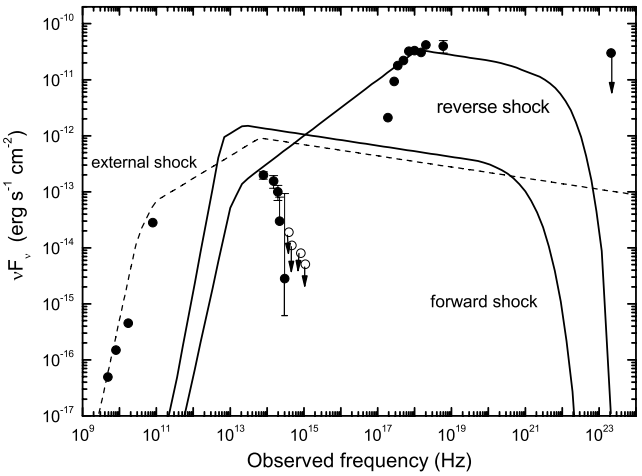

Figure 2. The broad-band spectral energy distribution of Swift J1644+57 at 2.9 d after the BAT trigger. The points show the observation data, which are taken from Bloom et al. (2011). The two solid lines represent the unabsorbed spectrum of the reverse and forward shocks, which are generated by the internal shock. The dashed line shows the spectrum of the external shock. In order to fit the spectrum, a moderate extinction ($A_V = 3$–5) is required.

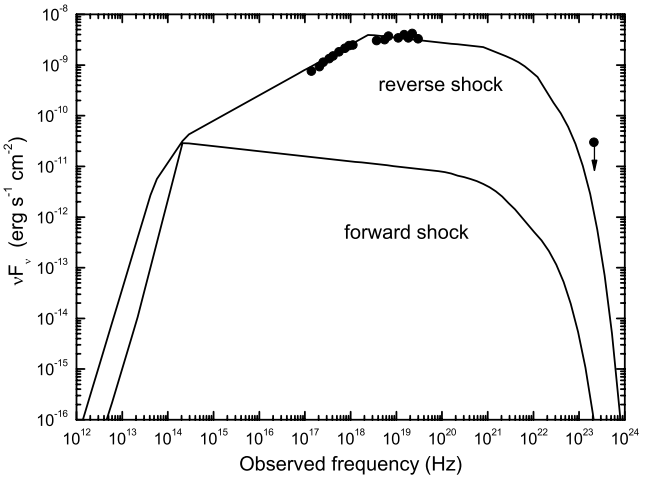

Figure 3. The spectral energy distribution of Swift J1644+57 at 31 h after the BAT trigger. The points show the observation data, which are taken from Burrows et al. (2011). The two lines represent the unabsorbed spectrum of the reverse and forward shocks, which are generated by the internal shock. The parameters of the two shocks are given in the text.

of extinction is reasonable in this case, because this event arises in the nucleus of the host galaxy. This value is also consistent with that determined by Bloom et al. (2011) and Burrows et al. (2011). Because of the large value of the synchrotron self-absorption frequency, the radio emission of the internal shock is suppressed. From observations, the radio emission is from a larger radius compared with the X-ray emission (Bloom et al. 2011; Burrows et al. 2011). The interaction between the first shell ejected by the central engine and the ISM results in an external shock. The radio emission is from large radius and can be modelled by this external shock, similarly to the GRB afterglow.

The total energy release during this initial period is about $E_{\rm iso} \sim 10^{53}$ erg (Bloom et al. 2011). The ISM density is about $n \sim 10\,{\rm cm}^{-3}$. Following Sari et al. (1998) and Bloom et al. (2011), we obtain the synchrotron frequencies and peak flux of the external shock as follows:

$$\begin{aligned} \nu_a &\simeq 2.0\times10^{10}\,{\rm Hz}\,\epsilon_{{\rm e},-1}^{-1}\epsilon_{B,-2}^{1/5}E_{53}^{1/5}n_1^{3/5},\\ \nu_m &\simeq 3.0\times10^{11}\,{\rm Hz}\,\epsilon_{{\rm e},-1}^{2}\epsilon_{B,-2}^{1/2}E_{53}^{1/2}t_{\rm days}^{-3/2},\\ \nu_c &\simeq 8.0\times10^{13}\,{\rm Hz}\,\epsilon_{B,-2}^{-3/2}E_{53}^{-1/2}n_1^{-1}t_{\rm days}^{-1/2},\\ F_{\nu,\rm max} &\simeq 170\,{\rm mJy}\,\epsilon_{B,-2}^{1/2}E_{53}n_1^{1/2}t_{\rm days}^{-3/4}d_{\rm L,27.7}^{-2}. \end{aligned} \quad (12)$$

The expression for $F_{\nu,\rm max}$ is a little different from that of Sari et al. (1998), because the observer has already observed the edges of the jet, as discussed in Bloom et al. (2011). The spectrum of the external shock is shown as a dashed line in Fig. 2, and can only produce a simple power law in the X-ray region. The radio light curve shows differences from the $t^{-5/3}$ behaviour observed in the late X-ray light curve (Giannios & Metzger 2011; Metzger, Giannios & Mimica 2011) because the radio light curve should be determined by the evolution of the external shock and has nothing to do with the accretion rate in the disc.

Our model therefore predicts that, during the high state (flaring), internal shock emission will dominate in the X-ray band and a broken power-law spectrum is shown. During the low state (no flares) there are no internal shocks and the emission is from the external shock. Because the typical frequencies of an external shock are low during the first few days (see equation 12), the spectrum in the X-ray band appears as a single power law if no energy injection happens. In both states, the radio emission is from the external shock.

In Fig. 3, we fit the spectrum data from Burrows et al. (2011) detected at the same period. We adopt the following parameters: $L_4 = L_1 = L = 10^{48.5}\,{\rm erg\,s^{-1}}$, $\gamma_4 = 1000$, $\gamma_1 = 10$, $\delta t = 100$ s, $\epsilon_{\rm e} = 0.8$ and $\epsilon_B = 0.001$. Since shocks produced by collisions are highly non-linear processes, the microscopic parameters, i.e. $\epsilon_{\rm e}$ and ϵ_B, can be different for different collisions.

The X-ray flux from Swift J1644+57 is observed to track the X-ray hardness (Bloom et al. 2011; Levan et al. 2011). The X-ray flux and photon index exhibit a strong anticorrelation. This signature is a natural consequence of our model. In the earlier stage when internal shocks dominate, the X-ray flux is high but variable and harder. At later times when the external shock dominates, the X-ray flux becomes lower but less fluctuating and softer.

The durations of flares are very complicated, similarly to X-ray flares in GRBs. For an individual flare, the duration can be roughly estimated as Δ/c, where Δ is the width of the shell (Maxham & Zhang 2009). If the ejecta come from the disc around a black hole, this should have the size $r_{\rm d} \sim 3r_s \sim 6GM/c^2 \sim 8\times10^{11}M_6$ cm, where M is the mass of the black hole. From the minimum rise time, Bloom et al. (2011) and Burrows et al. (2011) have estimated $M_6 \sim 10$. Thus the duration of an individual flare should be of the order of $\Delta/c \sim r_{\rm d}/c \sim 200$ s. However, flares can superimpose on each other if shells collide near the same time. For example, the duration of the flare detected at 111 045 s after the BAT trigger is about 300 s, which is consistent with the rise time-scale, but the duration of the flare at about 1.115×10^5 s after the BAT trigger with minimum rise time is longer than 1000 s. We believe that this flare is a superposition of several flares. It is interesting to note that the flares detected in GRBs indicate that the shell width Δ broadens with ejected time. A natural broadening mechanism is shell spreading. After a shell enters the spreading regime, the width of the shell is proportional to the radius, so that if the collision radius is larger the duration of the X-ray flare can be longer. In this event, we can also see that the width of flares broadens with ejected time. This is similar to some central engine models of GRBs: for example, in the fragmented disc model proposed by Perna et al.

(2006), clumps at larger radius have lower densities and tend to be more spread out so that the accretion time-scale is longer.

4 SUMMARY

In this paper we propose an internal shock model to explain the X-ray flares of Swift J1644+57. In the internal shock model, collisions between a series of relativistic shells generate many pairs of forward and reverse shocks. The synchrotron emission produced by the forward and reverse shocks can dominate in two quite different energy bands if the Lorentz factors of these two types of shock are significantly different from each other. We show that the spectral energy distribution of Swift J1644+57 could be fitted with an internal shock model in which the reverse shock is relativistic and the forward shock is Newtonian. A moderate extinction ($A_V = 3$–5) is required; this value is consistent with that used in Bloom et al. (2011) and Burrows et al. (2011). Burrows et al. (2011) showed that the high-frequency spectrum is produced by synchrotron and SSC mechanisms, similar to the Poynting-flux-dominated blazar jet model. The radio fluxes come from a larger region of the other jet. This model requires continuous *in situ* re-acceleration of electrons to maintain a low-energy cut-off in the electron distribution (Aliu et al. 2011). Bloom et al. (2011) presented two models for the spectrum: one is a two-component blazar emission model, the other is forward shock emission from jet–ISM interaction plus an EIC emission model. On the high-frequency side, however, the LAT and VERITAS upper limits require that the SSC component is suppressed by γ–γ pair production. The soft photons from the disc outflow may provide sources for γ–γ production.

The rapid rise and decline of the light curve may indicate an internal shock origin of these flares. With an external shock it is very hard to account for X-ray flares (Burrows et al. 2005; Fan & Wei 2005; Zhang et al. 2006). During the high state, internal shock emission will dominate in the X-ray band and a broken power-law spectrum is shown. During the low state, there is no internal shock and the emission is from an external shock. The spectrum in the X-ray band will be shown as a single power law if no energy injection happens. In both states, the radio emission is from the external shock.

ACKNOWLEDGMENTS

We thank the referee for detailed and very constructive suggestions that have allowed us to improve our manuscript. We also thank Drs Y. W. Yu and R. Li for useful discussion. KSC is supported by GRF Grants of the Government of the Hong Kong SAR under HKU 7011/10P. FYW is supported by the National Natural Science Foundation of China (grant no. 11103007), Jiangsu Planned Projects for Postdoctoral Research Funds 1002006B and China Postdoctoral Science Foundation funded projects (20100481117 and 201104521).

REFERENCES

Aliu A. et al., 2011, ApJ, 738, L30
Blandford R. D., McKee C. F., 1976, Phys. Fluids, 19, 1130
Blandford R. D., Znajek R. L., 1977, MNRAS, 179, 433
Bloom J. S. et al., 2011, Sci, 333, 203
Burrows D. N. et al., 2005, Sci, 309, 1833
Burrows D. N. et al., 2011, Nat, 476, 421
Campana S., Foschini L., Tagliaferri G., Ghisellini G., Covino S., 2011, GCN Circ., 11851
Cannizzo J. K., Troja E., Lodato G., 2011, ApJ, 742, 32
Cheng K. S., Lu Y., 2001, MNRAS, 320, 235
Cheng K. S., Wei D. M., 1996, MNRAS, 283, L133
Cummings J. R. et al., 2011, GCN Circ., 11823
Dai Z. G., Lu T., 2002, ApJ, 565, L87
Fan Y. Z., Piran T., 2008, Frontiers of Physics in China, 3, 306
Fan Y. Z., Wei D. M., 2005, MNRAS, 364, L42
Giannios D., Metzger B. D., 2011, MNRAS, 416, 2102
Huang Y. F., Cheng K. S., Gao T. T., 2006, ApJ, 637, 873
Kobayashi S., Piran T., Sari R., 1997, ApJ, 490, 92
Krolik J. H., Piran T., 2011, ApJ, 743, 134
Levan A. J. et al., 2011, Sci, 333, 199
Maxham A., Zhang B., 2009, ApJ, 707, 1623
Metzger B. D., Giannios D., Mimica P., 2011, preprint (arXiv:1110.1111)
Paczyński B., Xu G. H., 1994, ApJ, 427, 708
Panaitescu A., Kumar P., 2000, ApJ, 543, 66
Perna R., Armitage P. J., Zhang B., 2006, ApJ, 636, L29
Proga D., Zhang B., 2006, MNRAS, 370, L61
Rees M. J., Mészáros P., 1994, ApJ, 430, L93
Sakamoto T. et al., 2011, GCN Circ., 11842
Sari R., Piran T., 1995, ApJ, 455, L143
Sari R., Piran T., Narayan R., 1998, ApJ, 497, L17
Shao L., Zhang F. W., Fan Y. Z., Wei D. M., 2011, ApJ, 734, L33
Socrates A., 2011, preprint (arXiv:1105.2557)
Strubbe L. E., Quataert E., 2009, MNRAS, 400, 2070
Wijers R. A. M. J., Galama T. J., 1999, ApJ, 523, 177
Yu Y. W., Dai Z. G., 2009, ApJ, 692, 133
Yu Y. W., Wang X. Y., Dai Z. G., 2009, ApJ, 692, 1662
Zauderer B. A. et al., 2011, Nat, 476, 425
Zhang B., Mészáros P., 2002, ApJ, 566, 712
Zhang B. et al., 2006, ApJ, 642, 354

This paper has been typeset from a TEX/LATEX file prepared by the author.